# Influence of scale-breaking phenomena on turbulent mixing rates

Erwin George,* James Glimm,† Xiaolin Li,‡ Yuanhua Li,§ and Xinfeng Liu‖
*Department of Applied Mathematics and Statistics, Stony Brook University, Stony Brook, New York 11794-3600, USA*
(Received 14 June 2005; published 19 January 2006)

Simulations not seen before compare turbulent mixing rates for ideal fluids and for real immiscible fluids with experimental values for the surface tension. The simulated real fluid mixing rates lie near the center of the range of experimental values. A comparison to theoretical predictions relating the mixing rate, the bubble width, and the bubble height fluctuations based on bubble merger models shows good agreement with experiment. The ideal fluid mixing rate is some 50% larger, providing an example of the sensitivity of the mixing rate to physical scale breaking interfacial phenomena; we also observe this sensitivity to numerical scale-breaking artifacts.

DOI: 10.1103/PhysRevE.73.016304 PACS number(s): 47.27.−i, 47.11.−j

## I. INTRODUCTION

Turbulent mixing is an important but an unfinished subject. Acceleration driven mixing has been the subject of intense investigation over the past 50 years [1,2]. Idealized cases of steady acceleration (Rayleigh-Taylor or RT) and impulsive (Richtmyer-Meshkov or RM) mixing have been studied by theory [3,4], experiment [5–8], and numerical simulations [4,9–11], as documented in the proceedings of biannual conferences, e.g., [12,13]. The experiments occur in vastly different time and energy scales, the theories are generally ideal, with an absence of length scales, and the numerical simulations have scales set by mesh resolution, and ultimately by computer budgets and the decade in which the simulation is performed. Furthermore, not all relevant experimental scales (specifically the amplitude of the long wavelength initial perturbations) were recorded. In this context, efforts to compare theory, simulation, and experiment have been generally successful within a factor of 2, but the absence of a better agreement has led to alternate explanations regarding unresolved differences.

In this paper, we identify physical and numerical scale-breaking phenomena as significant contributors to turbulent RT mixing rates. We determine the influence of surface tension for immiscible fluids in the experiments of Read and Youngs [5,14] and Smeeton and Youngs [6] to have a 30% effect on the mixing rate. We have previously compared tracked and untracked numerical simulations and determined that numerical mass diffusion has a 100% or larger effect on the mixing rate, using typical levels of grid spacing [15]. Front tracking (FT) refers to a numerical algorithm that maintains a sharp interface description and is able to prevent numerical mass diffusion. Similar conclusions, formulated in terms of a Froude number analysis, are found in [11]. The influence of initial perturbations on the mixing rate has been argued previously [11].

*Electronic address: egeorge@ams.sunysb.edu
†Electronic address: glimm@ams.sunysb.edu
‡Electronic address: linli@ams.sunysb.edu
§Electronic address: yuali@ams.sunysb.edu
‖Electronic address: xfliu77@ams.sunysb.edu

We report here the results of a series of three-dimensional (3D) Rayleigh-Taylor simulations, based on an improved front tracking code [16]. The primary improvement is to use local grid based tracking, which greatly minimizes the interpolative smoothing of the interface during time steps which display interface bifurcation. The grid based algorithm previously used handles bifurcations robustly, but with excess interpolation, and now the grid based reconstruction is applied only in local regions where needed and not globally as before. The detailed comparison [16] documents the advantage of the current algorithm relative to the old, in reducing excess smoothing of the interface, and its advantages relative to other interface algorithms such as level sets [17] and volume of fluids [18] algorithms. Untracked simulations are by a total variation diminishing (TVD) algorithm. We have two primary results to report.

With no surface tension in the simulation, we find an increased mixing rate. The mixing rate is the coefficient $\alpha$ in the equation

$$h = \alpha A g t^2 \tag{1}$$

for the bubble height $h$, where the Atwood number $A$ is defined as $(\rho_2-\rho_1)/(\rho_2+\rho_1)$ and $g$ is the gravitational force. Acceptable experimental values are $\alpha=0.06\pm0.01$. For an ideal fluid flow, we find the value $\alpha=0.09$. However, using physical values of surface tension (for immiscible fluids from [5,6]), we find $\alpha=0.066$. The $h$ vs. $Agt^2$ plot has a straight line shape after an initial transient, and we here report the slope obtained by joining the initial to the final point; defining $\alpha$ in terms of the slope after the initial transient gives a slightly lower value 0.060. (Here we interpolate between adjacent simulations.)

## II. METHODS

We consider seven 3D experiments of Read [5] and six of Smeeton and Youngs [6], for which there are sufficient data to carry out the analysis, which are immiscible and which do not use surfactants. We infer a value of the initial wavelength $\lambda$ from the most unstable wavelength as determined theoretically from a dispersion relation. This value is compared to that obtained by counting numbers of bubbles at an early

 

TABLE I. Comparison of dimensionless surface tension determined by two different definitions of wavelength, theoretical ($\lambda_{th}$) and observational ($\lambda_o$).

| Experiment | Comment | Refs. | $\lambda_{th}$ (cm) | $\tilde{\sigma}_{th}$ | $\lambda_o$ (cm) | $\tilde{\sigma}_o$ |
|---|---|---|---|---|---|---|
| Read-Youngs | Immiscible [5] | No. 29 | 0.37 | $8.5\times10^{-3}$ | 0.45 | $5.7\times10^{-3}$ |
| Read-Youngs | Immiscible [5] | No. 35 | 0.39 | $8.5\times10^{-3}$ | 0.54 | $4.6\times10^{-3}$ |
| Smeeton-Youngs | Immiscible [6] | No. 104 | 0.42 | $8.5\times10^{-3}$ | 0.41 | $8.8\times10^{-3}$ |
| Smeeton-Youngs | Immiscible [6] | No. 105 | 0.45 | $8.5\times10^{-3}$ | 0.48 | $7.3\times10^{-3}$ |
| Smeeton-Youngs | Immiscible [6] | No. 114 | 0.43 | $8.5\times10^{-3}$ | 0.45 | $7.8\times10^{-3}$ |

time, related to the known dimensions of the container. This number is not precisely determined by this method, so the count was performed independently by three people and the results (not very different) were averaged. The resulting experimentally and theoretically determined wavelengths are mostly very similar in those cases where there is sufficient data to carry out the experimental determination. See Table I and Figs. 1 and 2.

We introduce the dimensionless surface tension $\tilde{\sigma}=\sigma/\lambda^2\Delta\rho g$, giving an initial $\tilde{\sigma}$ as presented in Table II. The experiments use a container 15 cm on an edge and have some 30 bubbles (varying between experiments) on the face of the container at an early time in the experiment, giving a bubble diameter $\lambda\approx15/30$ cm=0.5 cm. At the end of the experiment, the number of bubbles has decreased to about 6 across the face of the container, so that the dimensionless surface tension is 25 times smaller. For the simulation, we consider initial random modes with wave number 8–16, giving rise to about 12 bubbles along one edge of the computational domain, and thus representing a $5\times5$ cm$^2$ portion of the container, with $\tilde{\sigma}=11\times10^{-3}$. Other simulations start with $\tilde{\sigma}=10^{-2}$ and $7\times10^{-2}$. It ends with about 3 bubbles on a face, and $\tilde{\sigma}=6.7\times10^{-4}$. The simulation corresponds approximately to the first half of the experiment. The computational grid is $128^2\times512$. In [6], the theoretical wavelength is given by the dispersion relation $\lambda_{th}=2\pi(3\sigma/g\Delta\rho)^{1/2}$. Note that the dimensionless surface tension $\tilde{\sigma}_{th}=\sigma/\lambda_{th}^2\Delta\rho g=1/3(2\pi)^2=8.5\times10^{-3}$, for all values of $g$, $\lambda$, and $\Delta\rho$.

We compare these simulations to a typical untracked simulation (conducted previously [15]), see also [11]. Numerical mass diffusion in the untracked simulation reduces the time-dependent Atwood number and the observed value of $\alpha$, both by a factor of about 2 [15].

## III. RESULTS

Our principal result is the value for the mixing rate $\alpha$ for the bubble penetration into the heavy fluid. We compare these values to experiments and to a theoretical analysis based on a bubble merger model. In Fig. 1, we plot the bubble penetration height $h$ vs. $Agt^2$, for ideal and immiscible tracked simulations and ideal fluid untracked numerically diffusive simulations. The resulting slopes $\alpha$ are given in Table II.

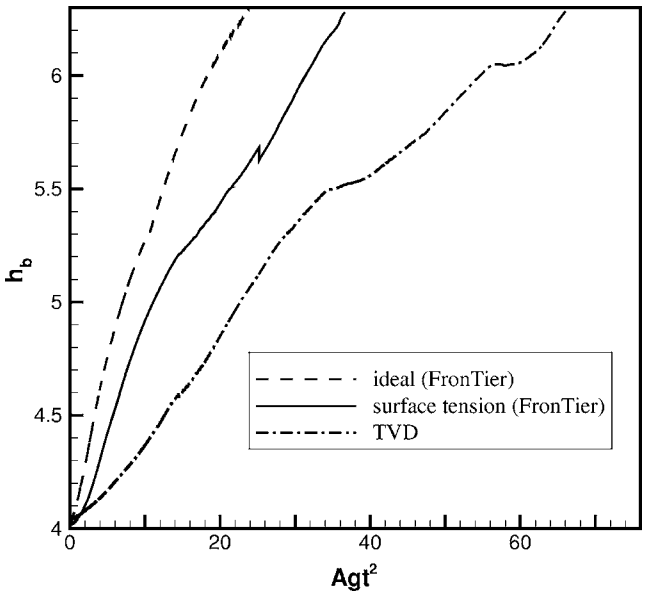


FIG. 1. The height of bubble penetration is contrasted for three simulations: Ideal fluids, tracked; real fluids (with surface tension), tracked; and ideal fluids, not tracked.

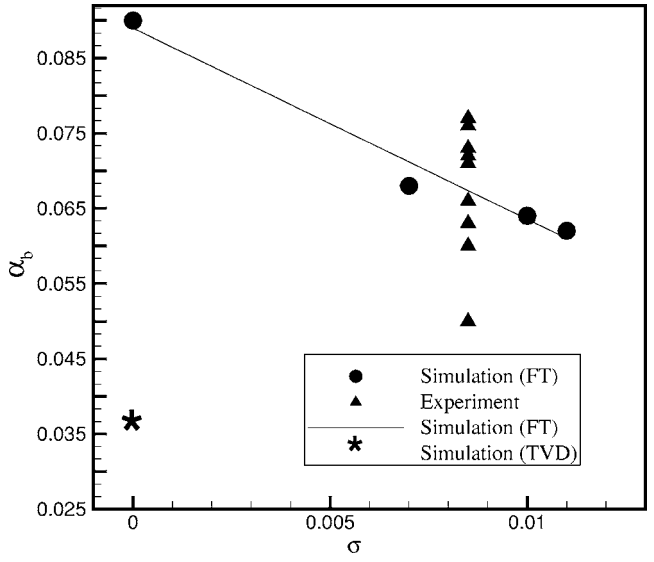


FIG. 2. The plot of mixing rates $\alpha_b$ vs. the dimensionless surface tension $\tilde{\sigma}_{th}$. The line represents the least squares fit to the FT simulation data. The TVD simulation disagrees with experiment by a factor of 2, a result typical of most untracked simulations.

TABLE II. Mixing rates compared: FronTier simulation compared to experiment and contrasted to untracked (TVD) and ideal fluid FronTier simulations. The two values for simulated $\alpha$ are the average slope and the final slope, $\tilde{\sigma}$ is determined by the theoretical wavelength $\lambda_{th}$.

| Experiment simulation | Comment | Refs. | $\alpha$ | $\tilde{\sigma}$ |
|---|---|---|---|---|
| Read-Youngs | Immiscible | [5] No. 29 | 0.073 | $8.5\times10^{-3}$ |
| Read-Youngs | Immiscible | [5] No. 33 | 0.066 | $8.5\times10^{-3}$ |
| Read-Youngs | Immiscible | [5] No. 35 | 0.071 | $8.5\times10^{-3}$ |
| Read-Youngs | Immiscible | [5] No. 39 | 0.076 | $8.5\times10^{-3}$ |
| Read-Youngs | Immiscible | [5] No. 58 | 0.077 | $8.5\times10^{-3}$ |
| Read-Youngs | Immiscible | [5] No. 60 | 0.073 | $8.5\times10^{-3}$ |
| Read-Youngs | Immiscible | [5] No. 62 | 0.063 | $8.5\times10^{-3}$ |
| Smeeton-Youngs | Immiscible | [6] No. 93 | 0.050 | $8.5\times10^{-3}$ |
| Smeeton-Youngs | Immiscible | [6] No. 97 | 0.060 | $8.5\times10^{-3}$ |
| Smeeton-Youngs | Immiscible | [6] No. 101 | 0.063 | $8.5\times10^{-3}$ |
| Smeeton-Youngs | Immiscible | [6] No. 104 | 0.066 | $8.5\times10^{-3}$ |
| Smeeton-Youngs | Immiscible | [6] No. 105 | 0.072 | $8.5\times10^{-3}$ |
| Smeeton-Youngs | Immiscible | [6] No. 114 | 0.060 | $8.5\times10^{-3}$ |
| Average | ±2 STD | | $0.067\pm0.015$ | |
| FronTier | Immiscible | | $0.062-0.055$ | $11\times10^{-3}$ |
| FronTier | Immiscible | | $0.064-0.058$ | $10\times10^{-3}$ |
| FronTier | Immiscible | | $0.068-0.061$ | $7\times10^{-3}$ |
| TVD | Ideal untracked | [15] | $0.035-0.034$ | 0.0 |
| FronTier | Ideal tracked | | $0.09-0.078$ | 0.0 |

The factor of 2 difference ($\alpha=0.067$ vs. 0.035) between experiment and untracked simulations is fully explained by the influence of the phenomena that introduce a length scale, and thus break the scale invariance of the Euler equations. That is the result of [15]. Scale breaking causes a lowering of $\alpha$ in simulations. An alternate explanation holds that the experiments have long wavelength initial perturbations, causing them to mix more rapidly than they would otherwise. The long wavelength perturbations, to the degree that they are present, cause an increase in experimental values of $\alpha$. These perturbations lower the simulation $\alpha$ required to agree with a hypothetical experiment lacking such perturbations. Both explanations must surely have a level of validity, but the relative importance of the two has been up to now an unresolved question. With the present agreement with experiment after the correction of scale dependent issues in the simulation, our results suggest that the factor of 2 discrepancy is resolved and that there is little room for further change from long wave perturbations beyond the scatter present in the experimental data. At least, these perturbations, to the degree that they are present in the experiments and affect mixing rates significantly, require some additional, and presently unknown, compensating corrections.

These two explanations, the scale effects vs. the long wavelength perturbations in the initial conditions, lead to different physical mechanisms regarding the primary physical processes governing observed turbulent mixing rates. With scale effects corrected, the primary physical mechanism is a bubble merger. With the continued increase in bubble size, the natural velocity of the rising bubbles increases. This leads to constant acceleration, and after the correction for the extra velocity associated with the fluctuating bubble height, to a bubble merger model [3], and the prediction of $\alpha=0.06$. The initial perturbation concept leads to the differential growth dynamics of initially imprinted perturbations as the primary mechanism for mixing rate acceleration.

TABLE III. Comparison of bubble radius and of height fluctuations between experimental data, theory, and simulation.

| Data/comment | $\alpha_b$ | $\alpha_r$ | $\alpha_{h_m}$ |
|---|---|---|---|
| Smeeton & Youngs [6] | 0.067 | 0.01 | 0.028 |
| Cheng *et al.* [3] | | | |
| Average No. 104, 105, 114 | | | |
| Formula (2) [3] | 0.0695 | | |
| RNG fixed point [3] | 0.06 | 0.01 | |
| FronTier immiscible | 0.062 | 0.01 | 0.034 |
| Formula (2) | 0.073 | | |

The bubble merger model, moreover, predicts a relation among three different measures of the mixing rate (three different $\alpha$'s). Thus we test this concept and the viability of bubble merger as a primary mechanism in mixing layer acceleration. The three $\alpha$'s are all coefficients of $Agt^2$; $\alpha=\alpha_b$ as in (1), refers to the bubble penetration height. $\alpha_r$ refers to the bubble radius, and $\alpha_{h_m}$ refers to the fluctuations in the bubble height. These three measures of the mixing zone growth rate are related by the formula

$$\alpha_b = \frac{1}{2}c_b\alpha_r^{1/2} + \left[\frac{1}{2k}+\frac{1}{2}\right]\alpha_{h_m}, \tag{2}$$

where $c_b=0.47$ is a Froude number associated with the terminal velocity of a single bubble and $k\approx0.51$ is a geometrical factor associated with the increase in bubble size due to bubble merger. See [3] for details.

To further test our simulations, we compare the three $\alpha$'s determined from our simulations to those measured from [6], as analyzed in [3] and to the relation (2), see Table III.

One might wonder why the bubble merger model agrees with the immiscible experimental value $\alpha=0.067\pm0.015$ rather than the ideal value $\alpha=0.09$ reported here. In fact, the envelope velocity used in [3] is a phenomenological model tested against the experimental data on immiscible fluids, see [19].

In order to carry out the simulation data analysis reported in Table III, we first record the local maxima of the interface between the two fluids, in a height range near the height of the leading bubble. The locations of these maxima are the bubble peaks of the simulation. We introduce Voronoi cells about these peaks to define the bubbles themselves (and including the associated spikes), as a decomposition of $x,y$ space. To select local maxima we want to avoid spurious maxima and identify distinct bubbles. For this purpose, we start with an arbitrary local maximum of the light fluid loca-

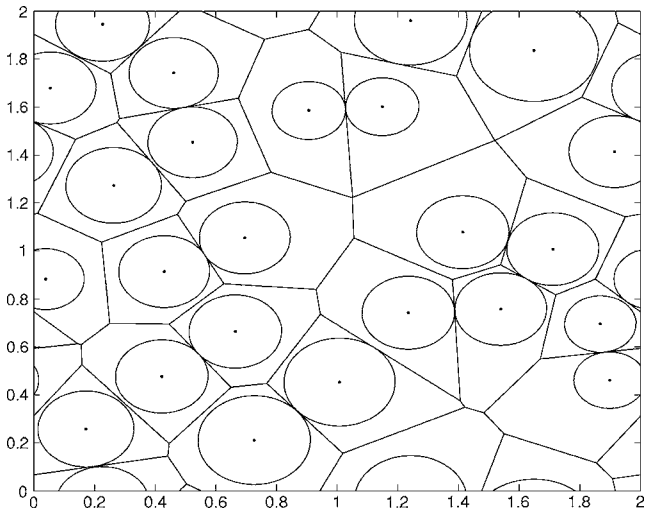


FIG. 3. Voronoi cell construction about the local bubble maxima to determine equivalent bubble radii based on a slice through the simulation at constant $z$ given by the volume fraction $\beta_{\text{light}}=0.2$.

tion, within the upper bubble strip defined by the volume fraction $\beta_{\text{light}} \leqslant 0.25$. This local maximum is accepted if it is unique within a $5 \times 5$ stencil of horizontal mesh blocks. In the case of competing maxima within this critical distance, the higher one is selected. This method of selecting local maxima and their heights also determines the height fluctuations of the bubbles. The value thus obtained was compared with that estimated by a manual inspection of the data, and the two were found to agree. For each bubble thus defined, we determine the curve defined by the intersection of the tracked surface with the hyperplane $z=$const, and an equivalent radius of a circle having equal area. From these data we find the average bubble radius at a given time. We also considered the radius of the largest circle contained within the cell. See Fig. 3 as an illustration of this construction. This definition gives too large a radius for the bubbles as it includes too much of the spike region between the bubbles; compare to Fig. 4 for the location of the light fluid through a fixed slice. We average the minimum and maximum radii for each bubble in this slice and average this over the bubbles to determine the average bubble radius; see Fig. 5 and Table III, which also show height fluctuations.

## IV. CONCLUSIONS

In this paper, we have reported on a set of 3D Rayleigh-Taylor chaotic mixing simulations, based on an improved tracking algorithm in the front tracking code FronTier. The real fluid simulations lead to agreement with experiment. Accurate numerical tracking to control numerical mass diffusion and accurate modeling of physical scale-breaking phenomena (surface tension) were the critical steps for this level of agreement. Remaining issues concern the role of surfactants and viscosity, which require additional physicial modeling. For miscible fluids, mass diffusion may be significant, and for all cases, a possible transition to turbulence may be important; see also the discussion of [20]. A sensitivity to

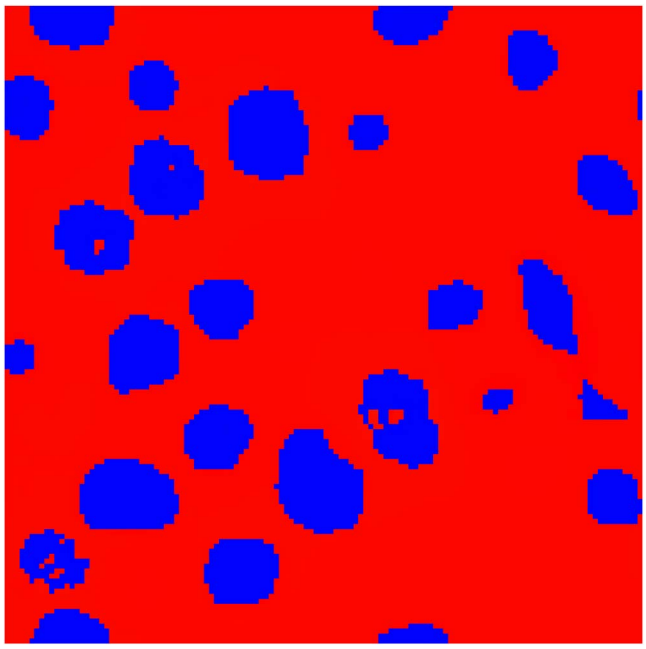

FIG. 4. (Color online) Horizontal cross section, showing the bubbles at a height given by the volume fraction $\beta_{\text{light}}=0.2$, for the same time step as in Fig. 3.

mesh resolution is a further issue to address as more powerful computers become available.

A broader conclusion of this paper is to document the sensitivity of Rayleigh-Taylor mixing rates to physical and numerical scale-breaking phenomena and to scale breaking diffusive or interface smoothing artifacts of the numerical algorithms used in simulations. Since the Rayleigh-Taylor phenomena occur on a variety of scales, from laser fusion to turbulent combustion in a supernova, the modeling of scale-breaking phenomena in the physics and eliminating it from the numerics becomes an issue.

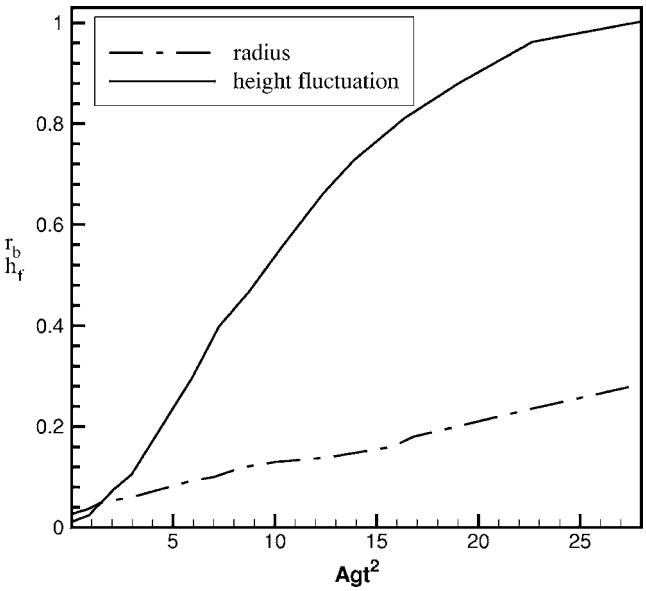


FIG. 5. Growth of mean bubble width ($r_b$) and bubble height fluctuations ($h_f$).

**ACKNOWLEDGMENTS**

This work was supported by Stony Brook University and supported in part by the NSF Grant No. DMS-0102480 and Los Alamos National Laboratory Contract No. 1481600105. This work was also supported by Brookhaven Science Associates, LLC, under Contract No. DE-AC02-98CH1-886 with the U.S. Department of Energy, by the U.S. Department of Energy Grant No. DE-FC02-01ER25461, and by the NSF Grant No. DMS-0102480. We would like to thank the many collaborators who have contributed to our simulation and modeling capabilities; especially Baolian Cheng, John Grove, and David H. Sharp for helpful discussions. We thank Stony Brook University, NERSC, and ORNL for access to the computational cycles used in this study.

[1] S. Chandrasekhar, *Hydrodynamic and Hydromagnetic Stability* (Oxford University Press, Oxford, 1961).
[2] D. H. Sharp, Physica D **12**, 3 (1984).
[3] B. Cheng, J. Glimm, and D. H. Sharp, Chaos **12**, 267 (2002).
[4] D. Oron, O. Sadot, Y. Srebro, A. Rikanti, Y. Yedvab, U. Alon, L. Erez, G. Erez, G. Ben-Dor, L. A. Levin, D. Ofer, and D. Shvarts,Laser Part. Beams **17**, 465 (1999).
[5] K. I. Read, Physica D **12**, 45 (1984).
[6] V. S. Smeeton and D. L. Youngs, Atomic Weapons Establishment Aldermaston Report No. 0 35/87 (1987) (unpublished).
[7] G. Dimonte and M. Schneider, Phys. Fluids **12**, 304 (2000).
[8] D. M. Snider and M. J. Andrews, Phys. Fluids **6**, 3324 (1994).
[9] R. L. Holmes, B. Fryxell, M. Gittings, J. W. Grove, G. Dimonte, M. Schneider, D. H. Sharp, A. Velikovich, R. P. Weaver, and Q. Zhang, J. Fluid Mech. **389**, 55 (1999).
[10] E. George, J. Glimm, X. L. Li, A. Marchese, and Z. L. Xu, Proc. Natl. Acad. Sci. U.S.A. **99**, 2587 (2002).
[11] G. Dimonte, D. L. Youngs, A. Dimits, S. Weber, M. Marinsk, S. Wunsch, C. Garsi, A. Robinson, M. Andrews, P. Ramaprabhu, A. C.Calder, B. Fryxell, J. Bielle, L. Dursi, P. MacNiece, K. Olson, P. Ricker, R. Rossner, P. F. Timmes, H. Tubo, Y. –N. Young, and M. Zingale, Phys. Fluids **16**, 1668 (2004).
[12] *Proceedings of the Third International Workshop on the Physics of Compressible Turbulent Mixing at Royaumont, France*, edited by D. Besnard, C. Cavailler, L. Dagens, P. Figeac, M. de Gliniasty, J. F. Haas, P. A. Holstein, J. Montigny, C. Parisot, and V. Rupert (CEA DAM, 1991).
[13] *Proceedings of the 4th International Workshop on the Physics of Compressible Turbulent Mixing*, edited by P. F. Linden, D. L. Youngs, and S. B. Dalziel (Cambridge University Press, Cambridge, England, 1993).
[14] D. L. Youngs, Physica D **12**, 32 (1984).
[15] E. George and J. Glimm, Phys. Fluids **17**, 1904 (1993).
[16] J. Du, B. Fix, J. Glimm, X. Li, Y. Li, and L. Wu, J. Comp. Phys. (to be published); Stony Brook University Report No. SUNYSB-AMS-05-02 (unpublished).
[17] X.-L. Li, Phys. Fluids A **5**, 1904 (1993).
[18] W. J. Rider and D. B. Kothe, J. Comput. Phys. **141**, 112 (1997).
[19] J. Glimm, X.-L. Li, R. Menikoff, D. H. Sharp, and Q. Zhang, Phys. Fluids A **2**, 2046 (1990).
[20] H. F. Robey, Phys. Plasmas **11**, 4123 (2004).